ACS APPLIED MATERIALS & INTERFACES

Research Article

www.acsami.org

Effects of Aging Temperature and Time on the Corrosion Protection Provided by Trivalent Chromium Process Coatings on AA2024-T3

Liangliang Li[‡] and Greg M. Swain*[,†,‡]

[†]Department of Chemistry and [‡]Department of Chemical Engineering and Materials Science, Michigan State University, East Lansing, Michigan 48824-1322, United States

ABSTRACT: The effects of aging temperature and time on the physical structure of and corrosion protection provided by trivalent chromium process (TCP) coatings on AA2024-T3 are reported. The TCP coating forms a partially blocking barrier layer on the alloy surface that consists of hydrated channels and or defects. It is through these channels and defects that ions and dissolved O_2 can be transported to small areas of the underlying alloy. Reactions initiate at these sites, which can ultimately lead to undercutting of the coating and localized corrosion. We tested the hypothesis that collapsing the channels and or reducing the number of defects in the coating might be possible through post-deposition heat treatment, and that this would enhance the corrosion protection provided by the coating. This was tested by aging the TCP-coated AA2024 alloys in air overnight at room temperature (RT), 55, 100, or 150 °C. The TCP coating became dehydrated and thinner at the high temperatures (55 and 100 °C). This improved the corrosion protection as evidenced by a 2× increase in the charge transfer resistance. Aging at 150 °C caused excessive coating dehydration and shrinkage. This led to severe cracking and detachment of the coating from the surface. The TCP-coated AA2024 samples were also aged in air at RT from 1 to 7 days. There was no thinning of the coating, but the corrosion protection was enhanced with a longer aging period as evidenced by a 4× increase in the charge transfer resistance. The coating became more hydrophobic after aging at elevated temperature (up to 100 °C) and with aging time at RT as evidenced by an increased water contact angle from 7 to 100 °C.

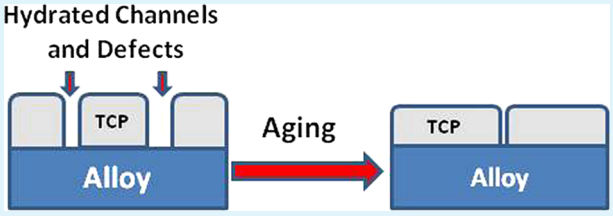

KEYWORDS: *trivalent chromium process coating, TCP, aging temperature, aging time, corrosion protection, AA2024*

INTRODUCTION

Chromate conversion coatings (CCCs) are widely applied to aerospace aluminum alloys to provide corrosion inhibition and to stabilize surface adhesion and electrical contact resistance.[1−3] These pretreatment coatings possess "self-healing" capability that provides active corrosion protection, for example, at a scratch. This occurs by release of soluble Cr(VI) into the adjacent solution and transport of this species to a nearby corroding site where it gets reduced to insoluble Cr(III) (e.g., $Cr(OH)_3$) to form a passivating layer.[4−8] Unfortunately, the active Cr(VI) species, chromate (CrO_4^{2-}), is a potent carcinogen and is highly toxic. Concerns about worker exposure and environmental pollution have stimulated efforts to develop alternate pretreatment coatings that contain no Cr(VI) but provide comparable corrosion protection to aluminum alloys.[2,3,9−11]

The trivalent chromium process (TCP) coating, originally developed at NAVAIR (U.S. Naval Air Systems Command, Patuxent River, Maryland), is a non-chromate conversion coating on the market.[1−3,11,12] TCP baths generally contain potassium hexafluorozirconate (K_2ZrF_6), chromium sulfate ($Cr_2(SO_4)_3$), and acid (HF), which produces a bath pH of 3.8−4.0.[1,7−11] Work has shown that the coating formation on AA2024 is initiated by attack of the surface by H^+ and F^- ions in the bath.[3,12] This attack causes dissolution of the passivating oxide layer and exposes the bare metal where cathodic reactions ensue (dissolved oxygen and hydrogen ion reduction) that cause the interfacial pH to increase. The increased interfacial pH drives hydrolysis of hexafluorozirconate (ZrF_6^{3-}) in the bath to a hydrated zirconia layer ($ZrO_2{\cdot}nH_2O$) that precipitates on top of a K_xAlF_{3+x} interfacial layer. Dardona *et al.* present data that indicate the film growth is likely due to fluoride ion sequestration by aluminum rather than alkaline hydrolysis. The sequestration of fluoride by aluminum (AlF_6^{3-}) liberates more zirconium ions (Zr^{4+}) that are prone to hydrolysis.[3] Preliminary measurements of the interfacial pH change during the coating formation on AA2024 have shown an increase from 3.8 to around 6.[14] Frankel et al. reported that the TCP coating also comprises some Al oxides (Zr−O−Al) in the interfacial layer.[15] The thickness of the biphasic coating has been confirmed by several groups to be around 100 nm on AA2024.[2,11,13,15] The coating provides corrosion protection to AA2024, 6061, and 7075, at least in part, by serving as a barrier layer.[11,13,15−17] Corrosion protection is evidenced by a charge transfer resistance, R_{ct}, that is 10−100× greater for the coated alloys as compared to the uncoated controls. The coating is stable with time and provides corrosion protection in aggressive chloride-containing electrolytes.[16,17] The coating appears to

Received: May 24, 2013
Accepted: July 11, 2013
Published: July 11, 2013

   dx.doi.org/10.1021/am4020023 | *ACS Appl. Mater. Interfaces* 2013, 5, 7923−7930

possess some hydrated channels and or defects through which ions and dissolved O_2 can be transported to localized regions of the underlying metal.

A question of interest is the following: is there any beneficial effect gained by aging the TCP coating after formation? In other words, can the defect density in the coating be reduced through controlled aging? In one of only two reports describing aging effects, Guo and Frankel showed that long-term (48 h) atmospheric aging produces small cracks in the TCP coating.[15] The authors, however, did not report how the corrosion protection was impacted by these coating alterations. We reported an interesting preliminary finding that atmospheric aging of TCP-coated AA2024 at room temperature (RT) for 72 h increased R_{ct} from ~10^5 to 10^9 ohm-cm^2.[13] This significant increase in R_{ct}, reflective of improved barrier properties, was only observed on a few of the coated samples tested.

To date, no systematic study has been conducted on how aging affects the physical structure and corrosion protection of TCP coatings on aluminum alloys. Herein, we address this knowledge gap by focusing on the following two questions:

(1) Is there any reproducible effect of the aging temperature and time on the physical structure and electrochemical properties (i.e., corrosion protection) of the TCP coating on AA2024?

(2) If there is a reproducible effect, then what is the associated mechanism?

EXPERIMENTAL SECTION

Reagents. All chemicals used were analytical grade quality or better. Sodium sulfate (Na_2SO_4) was purchased from CCI Chemical (Vernon, CA). The Turco 6849 and Turco Liquid Smut-Go NC solutions were provided by Henkel Corp. (Madison Heights, MI). Both were diluted with ultrapure water to 20% (v/v) before use. The TCP bath was Alodine 5900 RTU, also obtained from Henkel Corp., and was used as received. All solutions were prepared with ultrapure water (Barnstead) having a resistivity of >17 MΩ·cm.

Sample Preparation. Heat treated AA2024-T3 was used as the substrate for all tests. The standard chemical composition (ASM International) of this alloy is Cu (3.8−4.9 wt %), Mg (1.2−1.8 wt %), Mn (0.3−0.9 wt %), Fe (0.5 wt %), Zn (0.25 wt %), Ti (0.15 wt %), Cr (0.1 wt %), and Al (remainder). The metal samples were obtained as 2 mm-thick sheets. They were cut into 1 cm^2 squares and polished to a smooth surface. Mechanical grinding was performed wet on 1500 grit alumina sanding paper for 1 min. The samples were then fine-polished using 0.3 μm diam. alumina powder on a felt polishing pad, slurried with ultrapure water. The fine polishing lasted until a mirror-like finished was observed. Each polishing step was followed by a 20-min ultrasonic cleaning in ultrapure water to remove polishing debris. The polished samples were then degreased in 20% (v/v) Turco 6849 at 55°C for 10 min to remove any residual grease. This was followed by a 2-min rinse with tap water. The degreased samples were then deoxidized in 20% (v/v) Turco Liquid Smut-Go NC for 2 min at 23-27°C to form the TCP conversion coating. This was followed by another 2-min rinse with tap water. The deoxidizing solution is quite aggressive and causes alloy pitting. Finally, the cleaned and deoxidized samples were immersed in full strength Alodine 5900 RTU for 10 min at 21-27 °C. The coated samples were then rinsed with tap water for 2 min, and then air dried before any testing. The degreasing, desmutting and immersion coating times were selected based on the recommendation of the supplier for field application. The rinse with tap water was critical for reproducible coating formation and performance. We attribute this to the slightly more basic pH of our tap water (pH ~6.8) compared to the ultrapure water (pH ~5.8). The more basic pH likely leads to greater hydrolysis of the fluorozirconate precursors.

Electrochemical Measurements. All electrochemical measurements were conducted in a single-compartment glass cell using a CH Instruments potentiostat (Model CHI 650A, Austin, TX). The coated sample was mounted at the bottom of the cell with an o-ring defining the exposed geometric area (0.20 cm^2). The counter electrode was a Pt wire sealed in glass that was placed in a separate glass tube with a porous glass frit. The reference was an Ag/AgCl electrode (4 M KCl, E^0 = 0.197 V vs. NHE) that was housed in a Luggin capillary with a cracked glass tip. All measurements were made in air-saturated 0.5 M Na_2SO_4 at RT.

The electrochemical testing protocol was as follows: (i) measuring the open circuit or corrosion potential (E_{corr}) for 30 min; (ii) performing electrochemical impedance spectroscopy (EIS) analysis at E_{corr} from 10^5 to 10^{-2} Hz using a 10 mV rms AC sine wave; and (iii) recording a potentiodynamic cathodic scan from E_{corr} to a cathodic limit of −1.1 V vs Ag/AgCl, allowing the open circuit potential (OCP) to be re-established, and then an anodic scan from E_{corr} to 0.6 V vs Ag/AgCl. The potentiodynamic scans were recorded at 2 mV/s.

Two equivalent circuits were employed to fit the experimental data.[18] These are shown in Figure 1. The equivalent circuit in Figure 1A was used to fit the experimental data for the one-time-constant system (i.e., uncoated samples or coated samples with a significant defect density). R_e is the bulk electrolyte resistance. CPE_{dl} is a constant-phase element that represents the potential-dependent capacitance at the electrolyte-metal interface. R_{ct} is the charge transfer resistance for corrosion of the electrode surface. Figure 1B shows an equivalent circuit for an electrode that is conformally coated with a relatively low fraction of hydrated channels and or defects. Besides R_e, CPE_{dl}, and R_{ct} that represent the same parameters as in Figure 1A, R_{po} is the resistance of the electrolyte in the channels and defects. CPE_{co} represents the capacitance of the inert coating. A constant phase element is an equivalent electrical circuit component that models the behavior of a double layer that behaves as an imperfect capacitor. A CPE's impedance is mathematically given by $Z = 1/(Q\,(jw)^n)$ and the CPE resembles a capacitor with a phase shift angle of $-90° \times n$ rather than −90° for a perfect capacitor. The effective capacitance can be calculated using Q and n.[18,28]

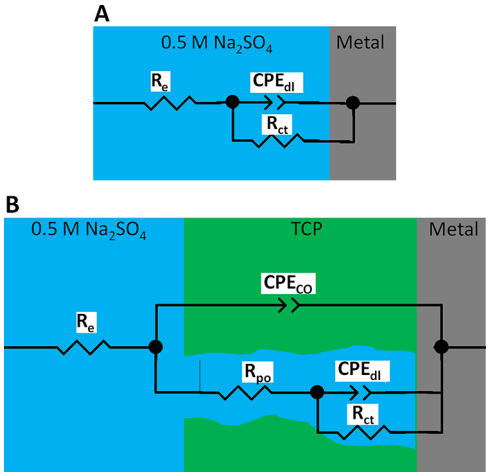

Figure 1. Equivalent circuits representing (A) an uncoated alloy surface or a surface coating with many defects and (B) a TCP coating on AA2024 with a low level of defects or hydrated channels.

Figure 2 shows the simulated phase shift vs log frequency plots generated using the equivalent circuit shown in Figure 1B. Most of the model values were held constant in the simulations (R_e, Q_{po}, n_{po}, Q_{dl}, and n_{dl}) except for the two that were varied: R_{po} and R_{ct}. As seen, the phase angle of the higher-frequency peak increases with increasing R_{po}. This indicates that the higher-frequency time constant is associated with the hydrated channels and defects of the coating. Similarly, the lower-frequency peak becomes wider with a maximum that shifts to lower frequency with increasing R_{ct}. This indicates that the lower-frequency time constant is associated with the underlying metal corrosion reaction.

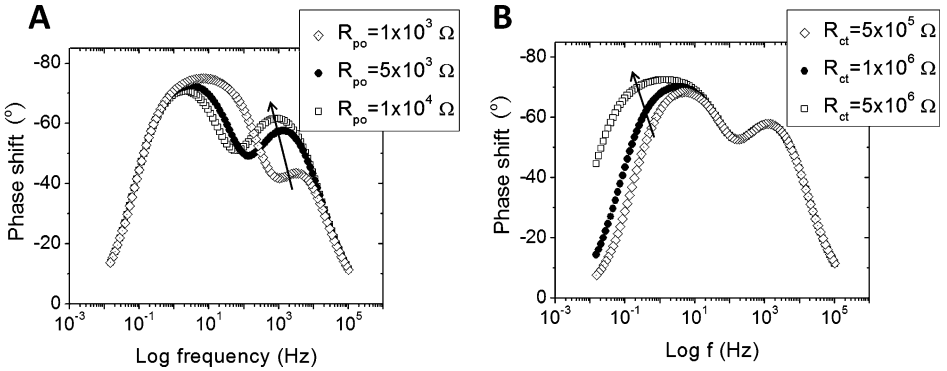

Figure 2. Simulated EIS spectra of phase shift vs. log frequency generated using the equivalent circuit shown in Figure 1B. The parameter values used in the simulation were R_e = 100 Ω, Q_{po} = 1 × 10^{-6} s^n/(Ω·cm^2), n_{po} = 0.85, Q_{dl} = 1 × 10^{-6} s^n/(Ω·cm^2),and n_{dl} = 0.85. Two values were varied: (A) R_{po} from 1 × 10^3 to 1 × 10^4 Ω and (B) R_{ct} from 5 × 10^5 to 5 × 10^6 Ω.

The corrosion current density (J_{corr}) at E_{corr} was determined by Tafel analysis of the slow-scan potentiodynamic *J-E* curve data.[19] For large cathodic overpotentials, the Butler–Volmer equation can be simplified to the following:

$$\log J = \log J_{corr} + (\eta/b_c) \quad (1)$$

where $\eta = E - E_{corr}$ is the cathodic overpotential, and b_c is the cathodic Tafel slope.

Electrochemical methods have been used to estimate the apparent porosity of coatings used to protect metal surfaces from corrosion.[20−22] We used the charge transfer resistances to estimate the apparent porosity of the TCP coating on the alloy, according to eq 2. The assumption in this treatment is that the coating is inert and that the corrosion rate of the coating is negligible compared to the corrosion rate of the alloy.[20−22]

$$P = (R_{ct,bare}/R_{ct,TCP}) \times 10^{(-|\Delta E_{corr}/b_a|)} \quad (2)$$

In the equation, $R_{ct,bare}$ and $R_{ct,TCP}$ are the charge transfer resistances of bare and TCP-coated substrate alloys, respectively; ΔE_{corr} is the difference of E_{corr} between the bare and TCP-coated alloys; and b_a is the anodic Tafel slope for the bare alloy. The apparent porosity calculated using this method reflects the relative fraction of hydrated channels and or defects that exist in the coating.

Characterization. Thermogravimetric analysis was carried out using an automated analyzer (TGA Q500, TA Instruments, Inc., TX). The powder samples were obtained by carefully scraping a TCP coating, aged overnight, from the metal surface. The temperature was varied from 25 to 450 °C at 10 °C/min under an N_2 flow of 20 mL/min. In some cases, the temperature was initially held at 120 °C for 30 min to desorb water prior to the variable temperature experiment.

Elements analysis (Al, Zr, and Cr) of the powder samples was performed using energy-dispersive X-ray spectroscopy (EDX). Results indicated that the scraped powder samples contained material from both the coating and the underlying alloy surface (e.g., Zr, F, O, and Al).

The thicknesses of the TCP coating and the Al oxide layer were determined using ex situ ellipsometry.[23] Ellipsometry has been used to investigate the thickness and optical properties of TCP coated on pure aluminum.[2,3] Ellipsometry measures the change in polarization state of linearly polarized light as a function of wavelength.[23] The measured parameters are the phase shift difference, Δ, and the amplitude ratio, tan Ψ, of the two orthogonally polarized components of the reflected wave (r_s and r_p). The parameters are defined through, tan (ψ) exp(iΔ) = r_p/r_s.[2,3,23] Our ellipsometric data were acquired on a VASE (J.A. Woollam Co., NE) instrument from 300 to 2500 nm. The optical constant and the coating thickness are extracted through a model-based analysis that describes the interaction of light with the film. The most commonly used model is the Cauchy equation:[2,3,23,24]

$$n(\lambda) = A + B/\lambda^2 + C/\lambda^4 \quad (3)$$

where n is the refractive index, λ is wavelength of incident light, and A, B, and C are the Cauchy fit parameters. During the modeling, a film thickness is first proposed. A computer algorithm adjusts the parameters (refractive index, n, and film thickness d) until reaching a low mean squared error (MSE). The ellipsometer employs more than one wavelength (193–2500 nm) to optimize the measurement of the physical properties of thin films.

The wettability of the TCP-coated AA2024 was assessed by measuring the static contact angle of ultrapure water on the coated samples.[25] One droplet (ca. 0.05 mL) of ultrapure water was dropped on the TCP-coated AA2024 surface, and its contact angle was measured using a video system (FTÅ200, First Ten Angstroms, Inc., VA).

RESULTS

Figure 3 shows the weight loss of a scraped TCP powder sample recorded by TGA during a temperature ramp from 25 to 450 °C under N_2. There is a small but progressive weight loss with temperature up to 290 °C and a more distinct 2% weight loss at temperatures above 290 °C. The first transient is attributed to desorption of water trapped within hydrated channels and or defects of the coating. The distinct weight loss at 290 °C is ascribed to the decomposition of hydroxides (e.g., CrOOH, or $Cr(OH)_3$) that are components of the coating.[26] The relatively low weight loss seen for the TCP coating is in stark contrast to the upwards of 30% weight loss seen for chromate conversion coatings when heated to temperatures up to 300 °C.[26] The dehydration observed at temperatures around 100 °C is of technical interest since this is within the service temperature range that TCP coatings experience in the field. Dehydration during ambient aging is a root cause for the loss of

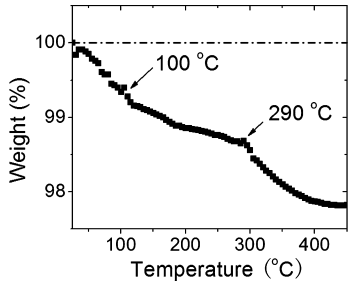

Figure 3. Weight loss measurement, under an N_2 atmosphere, of a TCP coating. The sample was obtained by carefully scraping the coatings from three TCP-coated AA2024 sample surfaces using a sharp blade.

dx.doi.org/10.1021/am4020023 | ACS Appl. Mater. Interfaces 2013, 5, 7923−7930

corrosion protection provided by chromate conversion coatings on aluminum.[26] In contrast, as seen below, dehydration of the TCP coating and the associated physical and chemical changes serve to enhance the corrosion resistance of the coating.

Figure 4A and B present charge transfer resistance (R_{ct}) and corrosion current density (J_{corr}) data, respectively, for TCP-coated and uncoated AA2024 samples. The data were recorded after aging the samples overnight (12−18 h) in ambient air at different temperatures. After overnight aging at RT and 55 °C, R_{ct} for the uncoated samples was 1.94 (± 0.23) × 10^5 and 1.42 (± 0.18) × 10^5 ohm-cm^2, respectively. These values are in the same range of those for a coated sample, 1.79 (± 0.22) × 10^5 ohm-cm^2 and 2.39 (± 0.35) × 10^5 ohm-cm^2, aged at RT and at 55 °C. This is attributed to formation of a more continuous and defect-free Al oxide layer. After aging at 100 °C, the R_{ct} values for the TCP-coated and uncoated samples became significantly different. The nominal R_{ct} for the coated sample was 3.72 (± 0.54) × 10^5 ohm-cm^2, which was about 2× greater than that of the uncoated sample, 1.19 (± 0.07) × 10^5 ohm-cm^2. Inversely, J_{corr} decreased by 2× as the temperature increased from RT to 100 °C. A noteworthy difference was observed for samples aged at 150 °C. R_{ct} decreased significantly to about 3.02 (± 0.22) × 10^4 ohm-cm^2; a value 2× smaller than the value for uncoated samples after aging at 150 °C and 10× smaller than the values at other temperatures. In contrast, for the uncoated samples, the nominal R_{ct} value decreased by 2× as the aging temperature increased from RT to 150 °C, 0.80 (± 0.10) × 10^5 ohm-cm^2, because of formation of more defective oxide films at high temperatures.[27] This R_{ct} value after aging at 150 °C is comparable to that for the uncoated samples right after deoxidizing (ca. 3 × 10^4 ohm-cm^2).[13] Consistent with this, J_{corr} increased by 10× for samples aged at 150 °C as compared to those at RT.

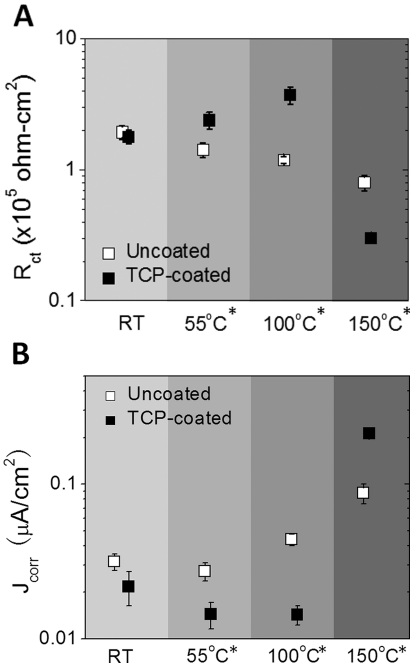

Figure 4. (A) Charge transfer resistance, R_{ct}, and (B) corrosion current density, J_{corr} data for the TCP-coated (■) and uncoated (□) AA2024 after overnight aging in air at varied temperatures: RT, 55, 100, and 150 °C. The measurements were conducted in air-saturated 0.5 M Na_2SO_4. Each datum is an average value of 3 samples.

Figure 5 presents the electrochemical impedance spectra for TCP-coated AA2024 after overnight aging at the different temperatures. Table 1 shows the best-fit parameters of the experimental data for RT, 55, and 100 °C to the equivalent circuit in Figure 1B, and the data for 150 °C to the one in Figure 1A. The phase-frequency profiles (Figure 5, right) show two distinct time constants (peaks) for the coated AA2024 aged at RT, 55, and 100 °C. The higher-frequency (~10^3 Hz) time constant arises from the hydrated channels and defects of the coating (R_{po}), while the lower-frequency (~10^0 Hz) time constant is associated with the corrosion of the underlying exposed metal (R_{ct}) (see Experimental Section). The high-frequency impedance R_{el}, as shown in the impedance-frequency profile (Figure 5, left), is essentially the bulk electrolyte resistance that is about 20 ohm-cm^2. R_{po} is the electrolyte resistance in the hydrated channels and or defects of the coating. The fact that that R_{po} increases with temperature up to 100 °C is consistent with a decreasing number of hydrated channels and or defects, or a shrinkage of the dimension of these. The R_{ct} values are consistent with the data in Figure 4 that were obtained from polarization curves. Q_{po} and n_{po} are mathematical parameters that are usually used to calculate the effective coating capacitance by $C_{po} = Q^{1/n}R^{1/n-1}$.[18,28] The C_{po} value decreases as the temperature increases from RT to 100 °C, which is mainly attributed to structural changes as shown in Figure 6.

Figure 6A presents data for the apparent porosity or defect parameter of the coating after overnight aging at the different temperatures. The hypothesis is that aging at elevated temperature dehydrates the coating causing it to shrink and become more continuous over the surface. The dimensions and

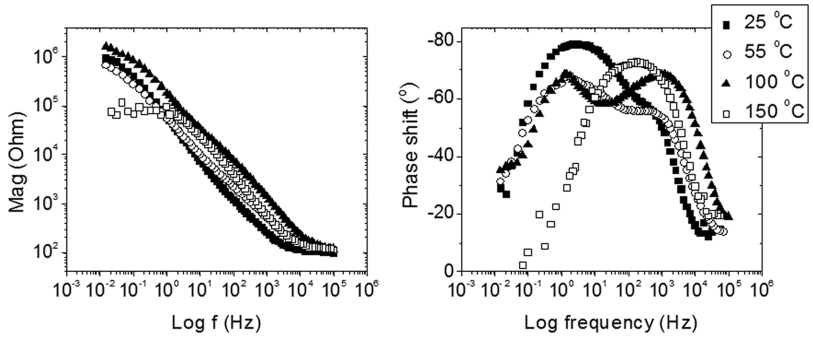

Figure 5. Bode plots for the TCP-coated AA2024 at E_{corr} after overnight aging at the various temperatures: RT (■), 55 (○), 100 (▲), and 150 °C (□). Three measurements were made in air-saturated 0.5 M Na_2SO_4.

Table 1. Best-Fit Parameters from Experimental EIS Results of the TCP-Coated AA2024 after Overnight Aging at Varied Temperatures: RT, 55, 100, and 150 °C[a]

temp (°C)	R_{el} (Ω·cm^2)	Q_{po} (×10^{-6} s^n/(Ω·cm^2))	n_{po}	C_{po} (μF/cm^2)	R_{po} (Ω·cm^2)	Q_{dl} (×10^{-6} s^n/(Ω·cm^2))	n_{dl}	R_{ct} (×10^5 Ω·cm^2)
RT	22	31.1	0.80	1.84	261	20.2	0.93	2.73
55	19	17.9	0.72	0.86	1.55 × 10^3	4.2	0.87	3.48
100	20	24.8	0.84	0.21	4.72 × 10^3	4.6	0.74	3.95
150	25					6.6	0.81	0.29

[a]The measurements were conducted in air-saturated 0.5 M Na_2SO_4 at RT.

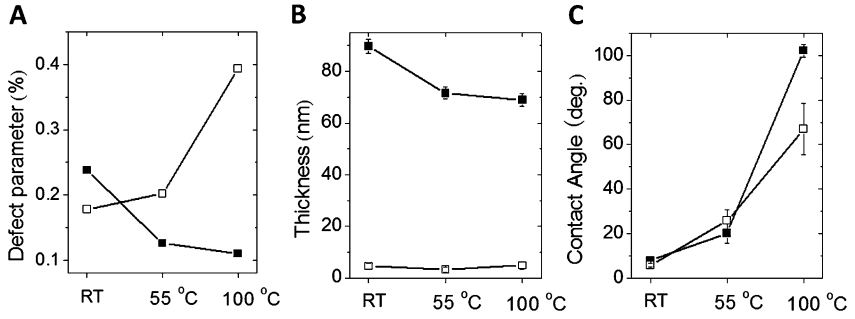

Figure 6. (A) Defect parameter, (B) coating thickness, and (C) contact angle of static water on the TCP-coated (■) and uncoated (□) AA2024 after overnight aging in air at various temperatures: RT, 55, and 100 °C. Each datum is an average of 3 measurements. The open squares in (B) represent the thickness of Al-oxide layers.

or number of hydrated channels and defects are expected to decrease. A more continuous and less defective coating would explain the increased R_{ct} values. The defect parameter, which is reflective of the fraction of hydrated channels and or defects, decreases modestly from 0.25 to 0.13% as the overnight-aging temperature increases from RT to 100 °C. Additionally, a more defect-free Al oxide layer likely forms on the exposed regions of the Al alloy where the channels and defects originally exist. Shrinkage or densification of the coating is evident in the ellipsometric data presented in Figure 6B. Clearly, the coating thickness decreases with aging temperature up to 100 °C. Figure 6C presents the static water contact angle for the TCP-coated alloy as a function of the aging temperature. The contact angle increases from 7.9 (± 1.3)° at RT, to 20.1 (± 4.3)° at 55 °C, and to 102.2 (± 2.8)° at 100 °C. As the coating becomes less hydrated and shrinks, the coating becomes more hydrophobic.

Changes in the roughness of the coating could be an explanation for time-dependent increase in the water contact angle. To study this, tapping-mode AFM images were recorded over 1 and 5 μm^2 dimensions of TCP-coated AA2024 panels. Panels were studied before and after (i) a 7-day age in air at RT and (ii) overnight aging in air at 55 °C. Even though the coating shows evidence for shrinkage, there was no change in the RMS surface roughness as the value ranged from 24−29 nm for all coatings, aged or unaged. Therefore, the change in wettability of the aged coatings is related to an altered chemical structure rather than an altered physical structure.

Figure 7 presents the effects of aging time at RT on the physical properties of the TCP coating. Figure 7A shows that the coating is about 90 nm thick at formation and remains the same thickness during the 7-day aging period. This thickness is consistent with other published data.[2,11,12,14] However, the static water contact angle increases gradually from 5.6 (± 1.8)° after overnight aging to 63.1 (± 0.3)° after 7-day aging, as shown in Figure 7B. Clearly, the coated surface becomes more hydrophobic with time, suggestive of a chemical change. The increase in hydrophobicity appears to be linked with the loss of

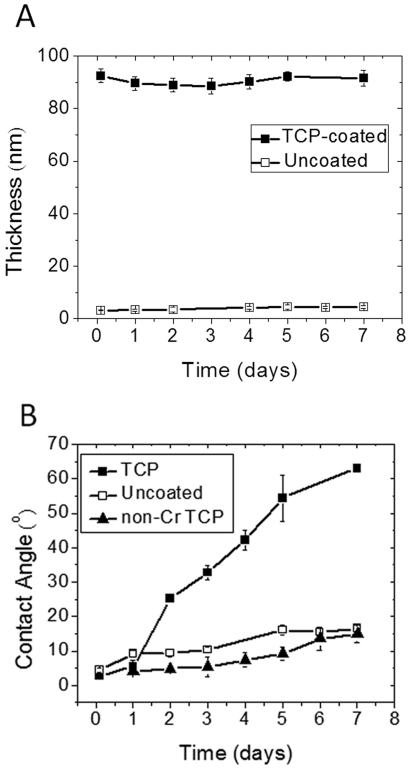

Figure 7. Effects of aging periods on the physical properties of the TCP-coated AA2024 during aging in air at RT: (A) thickness of TCP coatings for the coated samples (■) and that of Al oxide films for the uncoated samples (□), and (B) static contact angle for water on the uncoated (□), TCP-coated (■), and non-chromium conversion coated (▲) samples. Each datum is an average of 3 measurements.

weakly bound water. The loss of this weakly bound water and the associated structural change in the coating creates improved barrier properties to the transport of reactants through the coating. As is the case with chromate conversion coatings, the

dx.doi.org/10.1021/am4020023 | ACS Appl. Mater. Interfaces 2013, 5, 7923−7930

chemical change in the TCP coating maybe associated with the Cr(III) oxides.[26] This is evidenced by the much smaller water contact angle of the non-Cr TCP-coated alloy surface compared to that of the full TCP-coated surface throughout the whole 7-day aging, as seen in Figure 7B. Furthermore, a thin Al oxide film of several nanometers in thickness forms on the uncoated sample during aging at RT, as shown in Figure 7A. This also occurs at the bottom of the channels and defects in the TCP coating on the alloys, but only at the Al matrix sites. Therefore, the E_{corr} value shifts in the positive direction as the samples were aged for a longer period, as shown in Figure 8A.

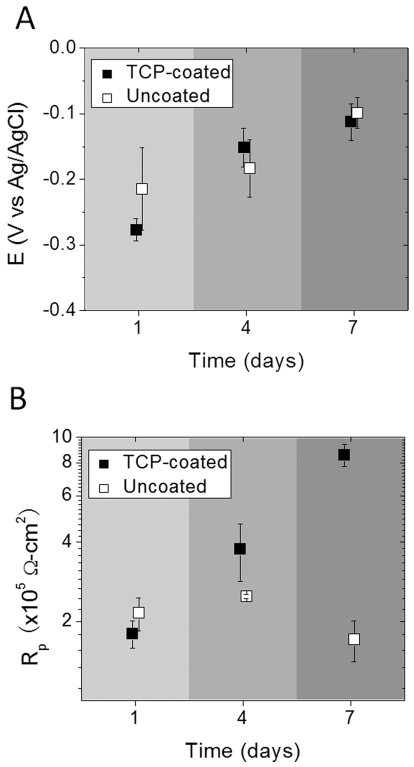

Figure 8. Effects of aging periods on the electrochemical properties of the TCP-coated (■) AA2024 during aging in air at RT: (A) E_{corr} and (B) R_{ct}. Data of the uncoated (□) is shown as control. Each datum is an average of 3 measurements.

A similar trend is also seen for the uncoated samples. Figure 8B shows the R_{ct} values for the TCP-coated and uncoated samples as functions of the aging period. The uncoated sample after 1-day aging exhibits an R_{ct} value (ca. 2×10^5 ohm-cm^2) that is about 10× greater than that right after deoxidization (ca. 3×10^4 ohm-cm^2). This is due to formation of an inert Al oxide film. The R_{ct} value stays relatively constant in this range through the entire 7-day aging period. In contrast, R_{ct} for the TCP-coated alloy increases by about 4×, from about 2×10^5 ohm-cm^2 after overnight aging to about 8×10^5 ohm-cm^2 after 7-day aging. This is attributed to dehydration of the coating, which reduced the number of defects and hydrated channels, as well as the formation of a more defect-free Al oxide film in those uncoated regions that restricts access of ions and dissolved O_2 to the metal surface.

■ DISCUSSION

Is There Any Reproducible Effect of the Aging Temperature and Time on the Physical Structure and Electrochemical Properties (i.e., Corrosion Protection) of the TCP Coating on AA2024? In summary, some modest reproducible benefits were found for aged TCP coatings. The physical and chemical properties of the coating were found to vary with the aging temperature and time, and both had an effect on the corrosion protection provided by the coating. For temperatures up to 100 °C, R_{ct} increases and J_{corr} decreases for the coated alloys because (i) the coating dehydrates and densifies reducing the number of hydrated channels and defects, and (ii) the growth of a more defect-free aluminum oxide layer on those exposed regions of the alloy. The increase in R_{ct} is a factor of 2 when comparing the performance of the coating aged at RT versus the coating aged at 100 °C. Dehydration occurs as the temperature increases (Figs. 2 and 6). The first dehydration step at temperatures centered around 100 °C is likely through evaporation of water trapped within channels and defects of the coating. With this loss of water, the coating becomes thinner. Consistent with the decrease in the number of hydrated channels and defects, the apparent porosity (i.e., defect parameter measure) of the coating decreases by about 2× after aging at 55 and 100 °C compared to that at RT (Figure 5A). The loss of water leads to shrinkage of the coating as the thickness, determined by ellipsometry, decreases from about 90 nm at RT to about 70 nm at 55 and 100 °C (Figure 5B). In addition, aging at elevated temperature (100 °C) also induces formation of a more defect-free Al oxide layer on the exposed areas of the alloy. This also contributes to a decrease in the apparent coating porosity and the increase R_{ct}. The coating also becomes progressively more hydrophobic with aging temperature as evidenced by the increasing static water contact angle from 7.9 ± 1.3 at RT to 102.2 ± 2.8 degrees at 100 °C (Figure 6C). We showed that this change in contact angle is largely due to the presence of Cr(III) in the coating as the same hydrophobic changes were not observed for hexafluorozirconate coatings devoid of Cr(III). In summary, overnight aging at up to 100 °C produces modest increases in the corrosion resistance of the coatings, as assessed from R_{ct} values, by a factor of two. Unfortunately, we did not observe any of the significantly increased in R_{ct} values (~10^9 ohm-cm^2) as was previously reported.[13] The decreased apparent porosity is an indication of fewer hydrated channels and defects as pathways for the transport of ions and dissolved O_2 to the underlying metal surface. The loss of weakly bound water and the associated structural changes of the coating give the coating improved barrier properties to the transport of reactants within the coating. This behavior is in stark contrast to what is observed with aged chromate conversion coatings.[26] It is well known that chromate conversion coatings exhibit a prompt loss in corrosion resistance when exposed to moderately elevated temperatures (60−100 °C).[26] They also suffer a gradual loss in corrosion resistance because of ambient temperature exposure. Dehydration is the root cause for the loss in corrosion resistance.[26]

Aging at 150 °C caused deleterious changes in the coating. At this temperature, significant coating dehydration occurs such that cracks form and sections of the coating detach from the surface. This exposes an increased fraction of the alloy surface to contact with the electrolyte solution. As a consequence, R_{ct} decreases to the same range as that for the bare sample (ca. 3×10^4 ohm-cm^2) right after desmutting. Clearly, aging at this elevated temperature is not recommended.

Besides the aging temperature, the aging time can affect the structure of the TCP coating and the corrosion protection it

provides on AA2024. With aging at RT, the coating thickness (Figure 7A) does not appear to change significantly but the wettability does. There is a progressive increase in the static water contact angle from 5.6 ± 1.8 at day 1 to 63.1 ± 0.3 degrees at day 7. Importantly, R_{ct} increases by 4× during this period from 2×10^5 to 8×10^5 ohm-cm^2. Frankel et al. reported possible shrinkage of the coating for long periods of atmospheric aging (48 h).[15] We did not observe any significant shrinkage, at least under our aging conditions (Figure 7A). Therefore, for aging time at RT, unlike the effects of aging temperature, a thinning or densification of the coating is not the explanation for the increased R_{ct}. We attribute the increased corrosion resistance to (i) growth of a more defect-free aluminum oxide layer on the exposed areas of the alloy and (ii) the increased hydrophobicity of the coating. Changes associated with the Cr(III) species cause the coating to become more hydrophobic over time. The new structure inhibits water from contacting the underlying metal surface.

If There Is a Reproducible Effect, Then What Are the Associated Mechanisms? For the coatings aged at elevated temperature, the 2× increase in R_{ct} is attributed to a reduction in the number of hydrated channels and defects because of (i) thinning of the coating due to dehydration, (ii) changes in the chemical nature of the Cr(III) species that make the coating more hydrophobic, and (iii) growth of a more defect-free aluminum oxide layer on the exposed regions of the alloy surface. For the coatings aged at RT for different periods of time, the 4× increase in R_{ct} occurs because of (i) changes in the chemical nature of the Cr(III) species that make the coating more hydrophobic and (ii) growth of a more defect-free Al oxide layer on the exposed regions of the alloy surface. We do not presently know what chemical bonding changes occur in the TCP coating with aging. However, we can gain some insight based on what is known about aged chromate conversion coatings. Buchheit et al. used the extended X-ray fine structure technique and found a shortening in Cr(III)−Cr(III) nearest neighbor distances upon dehydration of the Cr(III) oxide layer.[26] This leads to a short range structural rearrangement and polymerization of these Cr(III) oxides.[26,29] Finally, while the corrosion resistance of the TCP coating can be improved with aging, the more hydrophobic coating might be a problem for topcoat adhesion as many of the coatings used are aqueous-based. This point remains to be studied.

CONCLUSION

The effects of aging temperature and time on the electrochemical properties (i.e., corrosion resistance) of TCP coatings on AA2024-T3 were investigated. The TCP coating undergoes dehydration and condenses when aged at elevated temperatures. This along with the growth of a more defect-free aluminum oxide layer occurs during aging overnight at elevated temperature (≤ 100 °C). The coating also becomes progressively hydrophobic with the loss of water and associated chemical changes. All three contribute to the improved corrosion protection. However, aging at 150 °C causes excessive dehydration and shrinkage of the coating such that it undergoes severe cracking and even detachment from the metal surface. A longer aging period at RT enhances the corrosion resistance by 4× of the TCP-coated alloy by forming an aluminum oxide layer on the metal sites exposed in the coating channels and defects. The improvement in corrosion protection with aging at RT is also associated with increasing hydrophobicity of the coating. The best improvement in corrosion resistance was seen for coatings aged at RT for 7 days.

The work demonstrates that some benefits in terms of corrosion protection can be achieved by post-treatment of TCP-coated panels. What is unknown is how aging of the TCP coating affects the adhesion of primer layers or how it affects the performance of fully integrated systems (pretreatment conversion coating + primer + topcoat). Future work should include a systematic study of aging effects on other commercial TCP coating systems and on the corrosion status and adhesion of fully coated panels.

AUTHOR INFORMATION

Corresponding Author

*E-mail: swain@chemistry.msu.edu.

Notes

The authors declare no competing financial interest.

ACKNOWLEDGMENTS

The financial support provided by the Department of Navy through award #W912HQ-08-C-0011 is greatly appreciated. The authors also acknowledge the suggestions, guidance, and partnership of Professors Gerald Frankel and Rudy Buchheit (The Ohio State University), Dr. Mark Jaworowski (United Technologies), and the other team partners and consultants.

REFERENCES

(1) Iyer, A.; Willis, W.; Fruch, S.; Nickerson, W.; Fowler, A.; Bames, J.; Hagos, L.; Escarsega, J.; La Scala, J.; Suib, S. L. *Plat. Surf. Finish.* **2010**, *5*, 32−41.

(2) Dardona, S.; Jaworowski, M. *Appl. Phys. Lett.* **2010**, *97*, 181908−181910.

(3) Dardona, S.; Chen, L.; Kryzman, M.; Goberman, D.; Jaworowski, M. *Anal. Chem.* **2011**, *83*, 6127−6131.

(4) Akiyama, E.; Markworth, A. J.; McCoy, J. K.; Frankel, G. S.; Xia, L.; McCreery, R. L. *J. Electrochem. Soc.* **2003**, *150*, B83−B91.

(5) Clark, W. J.; McCreery, R. L. *J. Electrochem. Soc.* **2002**, *149*, B379−B386.

(6) Xia, L.; Akiyama, E.; Frankel, G. S.; McCreery, R. L. *J. Electrochem. Soc.* **2000**, *147*, 2556−2562.

(7) Ramsey, J. D.; McCreery, R. L. *J. Electrochem. Soc.* **1999**, *146*, 4076−4081.

(8) Zhao, J.; Frankel, G. S.; McCreery, R. L. *J. Electrochem. Soc.* **1998**, *145*, 2258−2264.

(9) Nickerson, W. C.; Lipnickas, E. *Proceedings of the 2003 Tri Service Corrosion Conference*, Las Vegas, NV, 2003.

(10) Berger, R.; Bexell, U.; Mikael-Grehk, T.; Homstrom, S.-E. *Surf. Coat. Technol.* **2007**, *202*, 391−397.

(11) Dong, X.; Wang, P.; Argekar, S.; Schaefer, D. W. *Langmuir* **2010**, *26*, 10833−10841.

(12) Matzdorf, C.; Kane, M.; Green, J. U.S. Patent Appl. 09/702,225, Patent # U.S. 6375726 B1, April 23, 2002.

(13) Li, L.; Swain, G. P.; Howell, A.; Woodbury, D.; Swain, G. M. *J. Electrochemical. Soc.* **2011**, *158*, C274−C283.

(14) Li, L.; Desouza, A. L.; Swain, G. M. *Analyst* **2013**, *138*, 4398−4402.

(15) Guo, Y.; Frankel, G. S. *Surf. Coat. Technol.* **2012**, *206*, 3895−3902.

(16) Guo, Y.; Frankel, G. S. *Corrosion* **2012**, *69*, 045002−1-045002-10.

(17) Li, L.; Doran, K.; Swain, G.M. *J. Electrochem. Soc.* **2013**, *160*, C396−C401.

(18) Orazem, M. E.; Tribollet, B. *Electrochemical Impedance Spectroscopy*, 1st ed.; Wiley-Interscience: Hoboken, NJ, 2008; pp 156−162.

(19) Bard, A. J.; Faulkner, L. R. *Electrochemical Methods*, 2nd ed.; Wiley: New York, 2000; pp 98−104.
(20) Tato, W.; Landolt, D. *J. Electrochem. Soc.* **1998**, *145*, 4173−4181.
(21) Creus, J.; Mazille, H.; Idrissi, H. *Surf. Coat. Technol.* **2000**, *130*, 224−232.
(22) Liu, C.; Bi, Q.; Leyland, A.; Matthews, A. *Corros. Sci.* **2003**, *45*, 1257−1273.
(23) Fujiwara, H. *Spectroscopic Ellipsometry: Principles and Applications*; Wiley: New York, 2007; p170.
(24) Campestrini, P.; Bohmb, S.; Schram, T.; Terryn, H.; De Wit, J. H. W. *Thin Solid Films* **2002**, *410*, 76−85.
(25) Mittal, K. L. *Contact Angle, Wettability and Adhesion*; CRC Press: Boca Raton, FL, 2006.
(26) Laget, V.; Jeffcoate, C. S.; Isaacs, H. S.; Buchheit, R. G. *J. Electrochemical. Soc.* **2003**, *150*, B425−B432.
(27) Jeurgens, L. P. H.; Sloof, W. G.; Tichelaar, F. D.; Mittemeijer, E. J. *J. Appl. Phys.* **2002**, *92*, 1649−1656.
(28) Lai, W.; Haile, S. M. *J. Am. Ceram. Soc.* **2005**, *88*, 2979−2997.
(29) Lin, X.; McCreery, R. L. *J. Electrochem. Soc.* **1998**, *145*, 3083−3089.